Electronic Supplementary Information

A general salt-resistant hydrophilic/hydrophobic nanoporous double layer design for efficient and stable solar water evaporation distillation

Yawei Yang,[a] Hongyang Zhao,[b] Zongyou Yin,[d] Jianqiu Zhao,[a] Xingtian Yin,[a] Na Li,[b] Dandan Yin,[b] Yannan Li,[b] Bo Lei,[b] Yaping Du*[bc] and Wenxiu Que*[a]

[a] Electronic Materials Research Laboratory, Key Laboratory of the Ministry of Education, International Center for Dielectric Research, and Shaanxi Engineering Research Center of Advanced Energy Materials and Devices, School of Electronic & Information Engineering, Xi'an Jiaotong University, Xi'an 710049, Shaanxi, China.

[b] Frontier Institute of Science and Technology, Xi'an Jiaotong University, Xi'an 710054, Shaanxi, China.

[c] School of Materials Science and Engineering, National Institute for Advanced Materials, Center for Rare Earth and Inorganic Functional Materials, Nankai University, Tianjin 300350, Tianjin, China.

[d] Research School of Chemistry, The Australian National University, Canberra, Australian Capital Territory 2601, Australia.

*Email: wxque@mail.xjtu.edu.cn (W. Que) ypdu2013@mail.xjtu.edu.cn (Y. Du)

Methods

Materials. $Cu(OAc)_2 \cdot H_2O$ (98.0%), $Zn(OAc)_2 \cdot 2H_2O$ (99.0%), $SnCl_2 \cdot 2H_2O$ (98.0%), cyclohexane (99.5%) and ethanol (99.7%) were purchased from Sinopharm. $Cu(Acac)_2$ (98.0%) and SeO_2 (99.4%) were purchased from Alfa-Aesar. Oleylamine (OLA, 70%) and Hexadecylamine (HDA, 90%) were purchased from Aldrich. All chemicals were used as received without further purification.

Synthesis of CZTSe and CTSe hierarchical nanospheres. For the synthesis of CZTSe nanospheres, 2 mmol $Cu(Acac)_2$, 1 mmol $Zn(OAc)_2 \cdot 2H_2O$, 1 mmol $SnCl_2 \cdot 2H_2O$, and 4 mmol SeO_2 (dissolved in 4 mL ethanol) were added into 40 mL OLA in a 100 mL three-neck flask on a Schlenk line. The mixture was degassed at 110 °C for 1 h, purged with N_2 for 30 min, and then heated to 280 °C for 1 h. The products were purified and washed with cyclohexane and ethanol through centrifugation at 8000 rpm for 5 min. The OLA-capped hydrophobic black powders were collected and dried at 60 °C under vacuum overnight. For the synthesis of CTSe nanospheres, 2 mmol $Cu(OAc)_2 \cdot H_2O$, 1 mmol $SnCl_2 \cdot 2H_2O$, and 3 mmol SeO_2 (dissolved in 3 mL ethanol) were added into 30 mL OLA and 10 g HDA in a 100 mL three-neck flask. The reaction was kept at 185 °C for 2 h. The remaining procedures were similar to those of CZTSe.

Characterizations. Crystalline properties of the samples were analyzed by a powder X-ray diffractometer (XRD, SmartLab, Rigaku, Japan) using Cu Kα radiation (40 kV,

30 mA), and a Raman spectrometer (Inviareflex, Renishaw, UK) equipped with a 514 nm laser. The morphologies of the samples were observed by a field emission scanning electron microscopy (SEM, Quatan 250FEG, FEI, USA), and a transmission electron microscopy (TEM, JEM-2100, JEOL., Japan). UV-Vis-NIR absorption spectra of the samples were measured by an ultraviolet/visble/near-infrared (UV/Vis/NIR) spectrometer (V-570, Jasco, Japan). Composition identification of the samples was performed by X-ray photoelectron spectroscopy (XPS, AXIS Ultrabld, Kratos, UK) using monochromatic Al Kα radiation (150 W, 15 kV, 1486.6 eV). All the binding energies of the samples were referenced to the C 1s peak (284.8 eV). The surface modification of the samples was characterized by the Fourier transform infrared spectroscopy (FTIR, Nicolet 6700, Thermo Scientific, USA) and contact angle meter (SL200KB, KINO Industry, USA).

First-principles calculations. The electronic structure and optical property were calculated within the density functional theory (DFT) as implemented in the CASTEP code. The projector augmented-wave (PAW) pseudopotentials were used with an energy cutoff of 400 eV for the plane-wave basis functions. The Brillouin zone integration was carried out using $4\times4\times2$ (for CZTSe) and $4\times2\times4$ (for CTSe) Monkhorst-Pack *k*-point meshes. The exchange-correlation functional, generalized gradient approximation (GGA) of Perdew-Burke-Ernzerhof (PBE) was used for initial structural relaxations, and the hybrid nonlocal exchange-correlation functional

(HSE06) was used to do the final structural relaxations and calculate the electronic structure and optical property.

Fabrication of solar evaporation device. Vacuum assisted filtration method was used to fabricate hierarchical nanospheres thin membranes with different loading mass. Briefly, CTSe or CZTSe cyclohexane dispersion containing known mass of hierarchical nanospheres (0.2, 0.4, 0.8, and 1.2 mg/cm^2) was filtrated through a commercial hydrophilic mixed cellulose ester filter membrane (0.22 μm in pore size, 5 cm in diameter, Shanghai Xinya Purification Equipment Co., China) by using Buchner funnel with sand core (4 cm in diameter). A thin black layer was stacked on top of the membrane, resulting in a hydrophilic/hydrophobic double layer. The commercial polystyrene foam and nonwoven fabrics were used as thermal insulating layer and water uptake path, respectively. The design and assembly process of the solar evaporation device are shown in Fig. 1a and Fig. S1, respectively. The hydrophilic layer of the double layer membrane was completely clinged to the nonwoven fabrics. To demonstrating the unique of the hierarchical nanospheres morphology, the CTSe nanoplates were also prepared and filtered on the membrane as the light absorber layer.

Water evaporation performance under one Sun. The hydrophilic/hydrophobic nanoporous double layer membrane was cut to 2×2 cm^2 for solar evaporation test. The as-fabricated solar evaporation device was allowed to float on the water surface in a teflon container under the irradiation of a 300 W Xe lamp (PLS-SXE300UV, Beijing

Perfectlight) equipped with a AM 1.5G filter (100 mW/cm^2) under an ambient temperature of 25~27 °C and a humidity of 30~40%. The temperatures of the vapor and upper bulk water were recorded by two thermocouples (placed on the top surface of the membrane and on the water, respectively). The temperature of the membrane was measured using an IR camera (VT04A, Fluke). The water weight change through evaporation was monitored by electronic analytical scale (BSA224S, Sartorius, 0.1 mg in accuracy), and then used to determine the evaporation rate and photothermal efficiency.

The solar thermal conversion efficiency (η) is estimated by

$$\eta = mh_{LV}/I \quad \text{(S1)}$$

where η is solar thermal conversion efficiency, m is the evaporation rate (the evaporation rate in dark field 0.276 kg/m^2 h should be subtracted to eliminate the effect of natural water evaporation), h_{LV} is the total enthalpy of sensible heat (Q, J/g) and phase change of liquid to water (L_v, J/g), and I is the solar illumination density (1 kW/m^2).

$$h_{LV} = Q + L_v$$

$$L_v = 1.91846 \times 10^3 [T_i/(T_i - 33.91)]^2 \text{ J/g}$$

$$Q = c\,(T_s - T_i) \text{ J/g} \qquad c = 4.2 \text{ J/g K}$$

L_v is dependent on the temperature (T_i) of the water/air interface where the vaporization occurs.[1] Q is calculated from the specific heat of water and the temperature difference between the source water (T_s) and water/air interface (T_i). Therefore, the temperature of the water/air interface (T_i) affects the values of both L_v

and Q, and further affects the calculation of η.[2] In our case, we take $h_{LV} = L_v + Q$ = 2256 J/g. This value of h_{LV} was found in multiple resources[3-8] which is why we used it in order to make our data comparable.

References

1. B. Henderson-Sellers, *Quart. J. R. Met. Soc.*, 1984, **110**, 1186-1190.
2. Y. Shi, R. Li, Y. Jin, S. Zhuo, L. Shi, J. Chang, S. Hong, K. Ng, and P. Wang, *Joule*, 2018, **2**, 1-16.
3. Y. Yang, X. Yang, L. Fu, M. Zou, A. Cao, Y. Du, Q Yuan and C. Yan, *ACS Energy Lett.*, 2018, **3**, 1165-1171.
4. R. Li, L. Zhang, L. Shi and P. Wang, *ACS Nano*, 2017, **11**, 3752-3759.
5. P. Zhang, J. Li, L. Lv, Y. Zhao and L. Qu, *ACS Nano*, 2017, **11**, 5087-5093.
6. X. Yang, Y. Yang, L. Fu, M. Zou, Z. Li, A. Cao and Q. Yuan, *Adv. Funct. Mater.*, 2018, **28**, 1704505.
7. L. Zhang, B. Tang, J. Wu, R. Li and P. Wang, *Adv. Mater.*, 2015, **27**, 4889-4894.
8. X. Gao, H. Ren, J. Zhou, R. Du, C. Yin, R. Liu, H. Peng, L. Tong, Z. Liu and J. Zhang, *Chem. Mater.*, 2017, **29**, 5777-5781.

The analysis of heat loss.

The heat loss of the solar evaporation device consists of three parts: (a) radiation, (b) convection, and (c) conduction.

a. Radiation:

The radiation loss can be calculated by the Stefan-Boltzmann equation.

$$Q_{rad} = \varepsilon A\sigma(T_1^4 - T_2^4) \quad \text{(S2)}$$

Where Q_{rad} denotes heat flux, ε is the emissivity (It is assumed that the absorber has a maximum emissivity of 0.97), A is the surface area (4 cm^2), σ is the Stefan-Boltzmann constant (5.67×10^{-8} W m^{-2} K^{-4}), T_1 is the average surface temperature (≈41 °C) of absorber at steady state condition, and T_2 is the ambient temperature (≈35 °C) upward

the absorber under the illumination of 1 Sun solar flux. According to equation (S2), the radiation heat loss is calculated to be ~4.0%.

b. Convection:

The convective heat loss is defined by Newton' law of cooling.

$$Q_{conv} = hA(T_1\text{-}T_2) \quad \text{(S3)}$$

Where Q_{conv} represents the heat energy, and h is the convection heat transfer coefficient (set as 5 W m^{-2} K)[1-6]. According to equation (S3), the connection heat loss is calculated to be ~3.0%.

c. Conduction:

$$Q_{cond} = Cm\Delta T \quad \text{(S4)}$$

Where Q_{cond} is the heat energy, C is the specific heat capacity of water (4.2 kJ $^oC^{-1}$ kg^{-1}), m is the water weight (8 g), and ΔT is the average increased bulk water temperature after 1 h illumination of 1 Sun solar flux (≈1 ^{o}C). According to equation (S4), the conduction heat loss is calculated to be ~2.3%.

References

1. P. Zhang, Q. Liao, T. Zhang, H. Cheng, Y. Huang, C. Yang, C. Li, L. Jiang and L. Qu, *Nano Energy*, 2018, **46**, 415-422.
2. Y. Yang, R. Zhao, T. Zhang, K. Zhao, P. Xiao, Y. Ma, P. M. Ajayan, G. Shi and Y. Chen, *ACS Nano*, 2018, **12**, 829-835.
3. X. Yang, Y. Yang, L. Fu, M. Zou, Z. Li, A. Cao and Q. Yuan, *Adv. Funct. Mater.*, 2018, **28**, 1704505.
4. N. Xu, X. Hu, W. Xu, X. Li, L. Zhou, S. Zhu and J. Zhu, *Adv. Mater.*, 2017, **29**, 1606762.
5. X. Li, R. Lin, G. Ni, N. Xu, X. Hu, B. Zhu, G. Lv, J. Li, S. Zhu and J. Zhu, *Natl. Sci. Rev.*, 2017, **0**, 1-8.
6. Y. Yang, X. Yang, L. Fu, M. Zou, A. Cao, Y. Du, Q Yuan and C. Yan, *ACS Energy Lett.*, 2018, **3**, 1165-1171.

Solar seawater desalination and water remediation. The seawater desalination and water remediation applications of the solar evaporation device were demonstrated by using real seawater (Bohai Sea, salinity ~2.75%; Qinghai Lake, salinity ~2.30%; and Caka Salt Lake, salinity ~32.2%) and simulated wastewater (organic dye aqueous solution: 10 mg/L Rhodamine B (RhB), 20 mg/L methyl orange (MO) and 20 mg/L methyl blue (MB); heavy metal aqueous solution: 1.0 mM $FeCl_3$, 0.1 M $CuCl_2$ and 0.5 mM $K_2Cr_2O_7$; bacterial culture suspension: 10^6 *Escherichia coli* and *Staphylococcus aureus*). The salinities (Na^+, K^+, Mg^{2+} and Ca^{2+}) of water before and after solar desalination were collected and tracked by inductively coupled plasma spectroscopy (ICP-OES, Optima 8000, PerkinElmer Instruments, 0.01 mg/L in accuracy). The decoloration efficiency of organic dyes and colored heavy metals before and after solar evaporation were collected and monitored by the UV/Vis/NIR spectrometer. The anti-bacteria efficiency was tested by culturing the water collected before and after solar evaporation.

For illustrating the salt (solute) blocking function and high stability of the hydrophobic surface, the hydrophobic ligands of hierarchical nanospheres were removed. Then the hydrophobic and hydrophilic samples were conducted the solar seawater (Bohai Sea) desalination for 10 hours.

Freshwater evaporation and collection under natural sunlight. An all-in-one solar distillation set-up (Fig. 5k) was designed and fabricated by polymethyl methacrylate (PMMA). The PMMA was treated with O_2-plasma to obtain the hydrophilic surface

for condensed water collection. 4 pieces of CTSe hydrophilic/hydrophobic nanoporous double layer membranes (4 cm in diameter) were used to distill freshwater from seawater (Bohai Sea) under natural sunlight for 8 h (9:00-17:00, June 27th, 2017, in Xi'an, China).

Vapor pressure and chemical potential decrease with the increase of the solutes concentration in water.

In equilibrium solution, the total vapor pressure of the solution can be determined by combining extended Raoult's law[1,2] and Dalton's law[3] by:

$$P = \sum_i \gamma_i P_i x_i \qquad \sum_i x_i = 1$$

Where P is the total vapor pressure of the solution, γ_i is the activity coefficient of the pure component i, P_i is the vapor pressure of the pure component i, x_i is the mole fraction of the component i in the solution. If a non-volatile salt (extremely low P_i) is dissolved into a solvent to form a solution, the P of the final solution will be lower than that of the solvent. Therefore, the vapor pressure as well as evaporation rate decreases with the increase of salt concentration x_i and decrease of the activity coefficient γ_i. In ideal solution, the activity coefficient $\gamma = 1$. Seawater is not an ideal solution, the activity coefficient of main salts in seawater $\gamma_{NaCl} \approx 0.66$, $\gamma_{Na2SO4} \approx 0.35$, $\gamma_{MgCl2} \approx 0.46$, $\gamma_{CaCl2} \approx 0.45$, $\gamma_{Mg2SO4} \approx 0.15$, $\gamma_{Ca2SO4} \approx 0.14$, $\gamma_{NaHCO3} \approx 0.62$, $\gamma_{Na2CO3} \approx 0.35$, $\gamma_{MgCO3} \approx 0.15$ and $\gamma_{CaCO3} \approx 0.14$ were calculated by using Pitzer model and Monte Carlo simulations at 25 °C and salinity 35.[4] They are indeed far from unity. In fact, the vapor pressure of salty water is lower than that of pure water.

The chemical potential is given by:

$\mu_i = \mu_i^\circ + RT*\ln \gamma_i x_i$

where μ_i° is the chemical potential of pure component i, γ_i is the activity coefficient of the pure component i, and x_i is the mole fraction of the component i in the solution. Therefore, the chemical potential of water decreases with the increase of solutes concentration x_i.

References

1. F. M. Raoult, Loi générale des tensions de vapeur des dissolvants (General law of vapor pressures of solvents), *Comptes rendus*, 1887, **104**, 1430-1433.
2. J. M. Smith, H. C. Van Ness and M. M. Abbott, Introduction to Chemical Engineering Thermodynamics (seventh ed.), New York: McGraw-Hill, 2005, 545.
3. J. Dalton, "Essay IV. On the expansion of elastic fluids by heat," *Memoirs of the Literary and Philosophical Society of Manchester*, 1802, **5**, 595-602.
4. A. Ulfsbo, Z. Abbas and D. R. Turner, *Mar. Chem.*, 2015, **171**, 78-86.

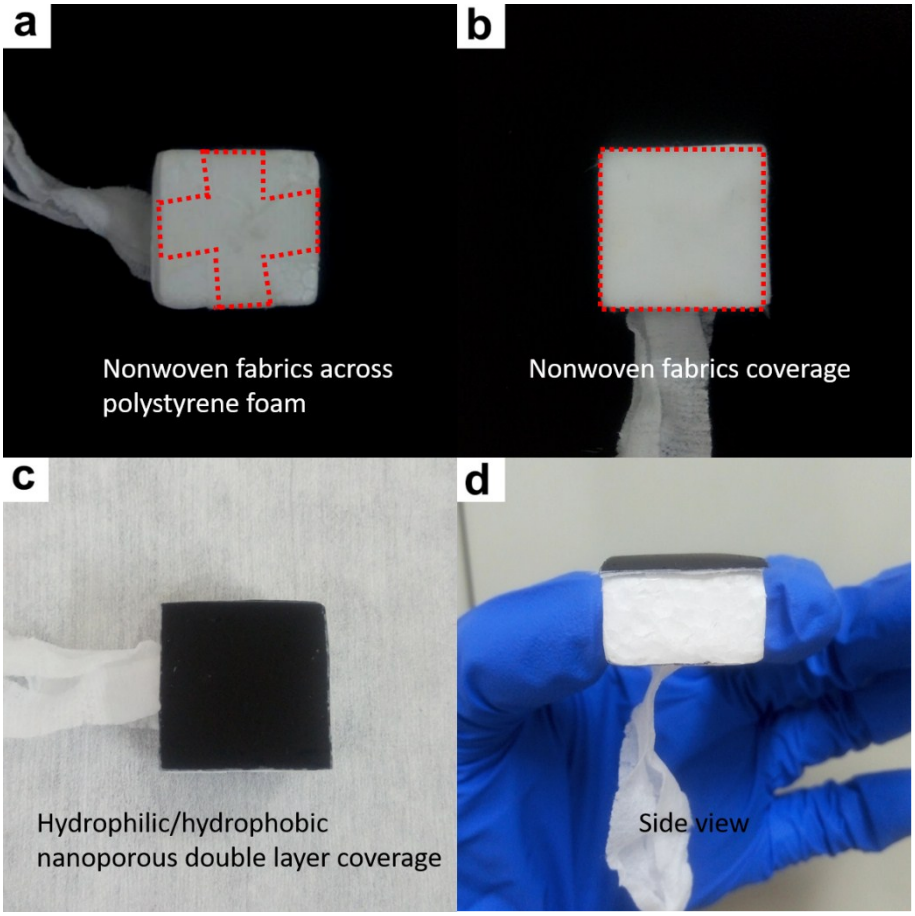

Fig. S1. Optical photos of the assembly process of the solar desalination device.

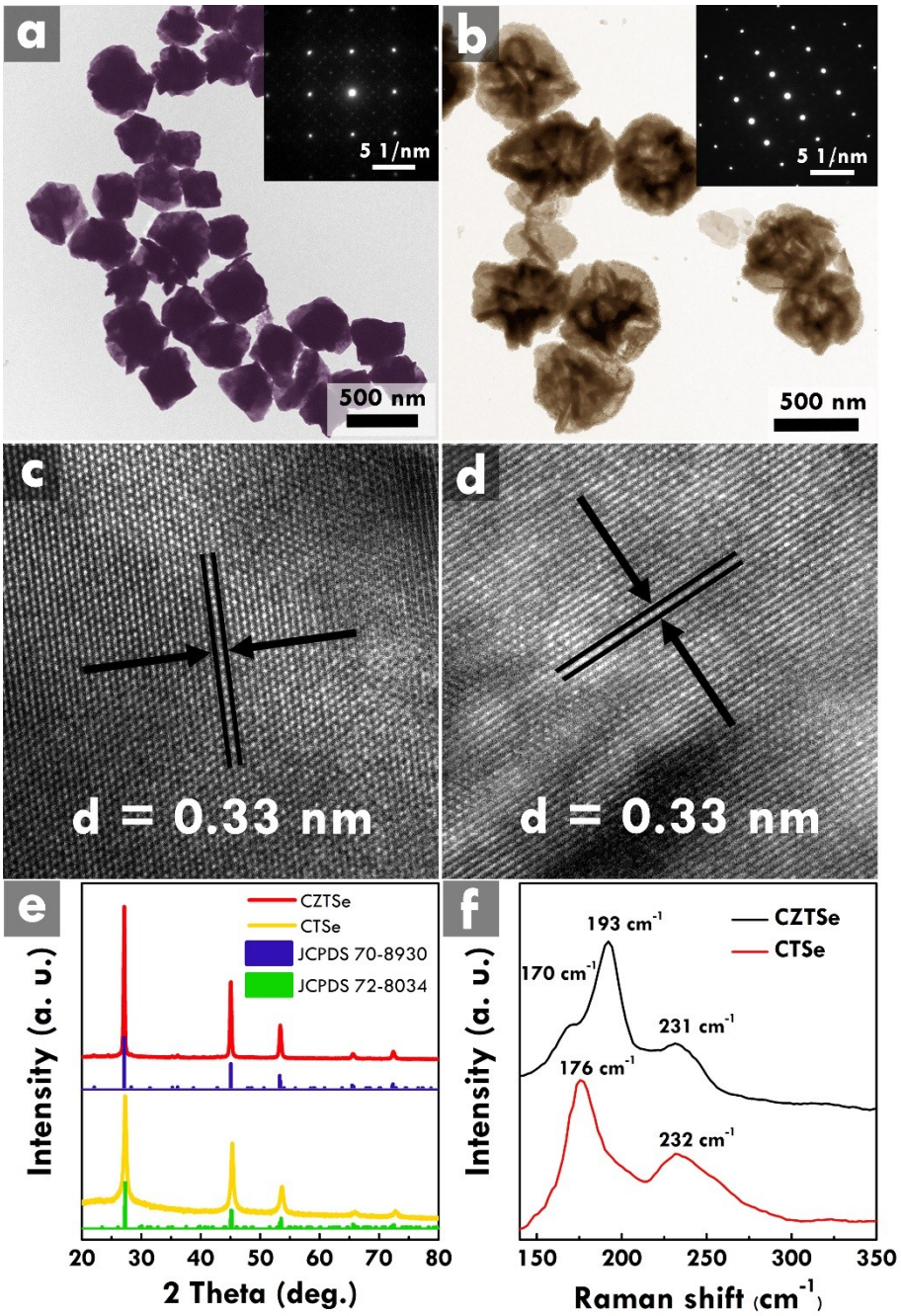

Fig. S2. TEM and HRTEM images of (a, c) CZTSe and (b, d) CTSe hierarchical nanospheres (insets of a and b: the corresponding SAED patterns of a single nanosphere). (e) XRD patterns and (f) Raman spectra of CZTSe and CTSe hierarchical nanospheres.

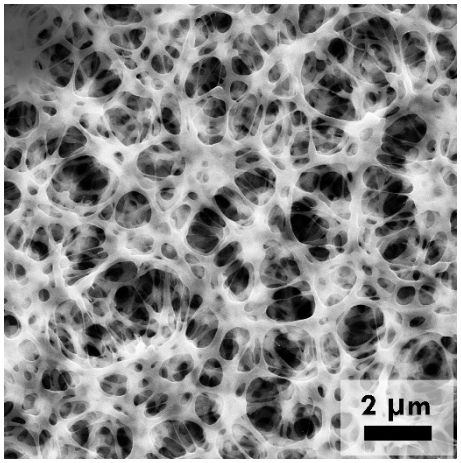

Fig. S3. SEM image of the hydrophilic mixed cellulose ester filter membrane.

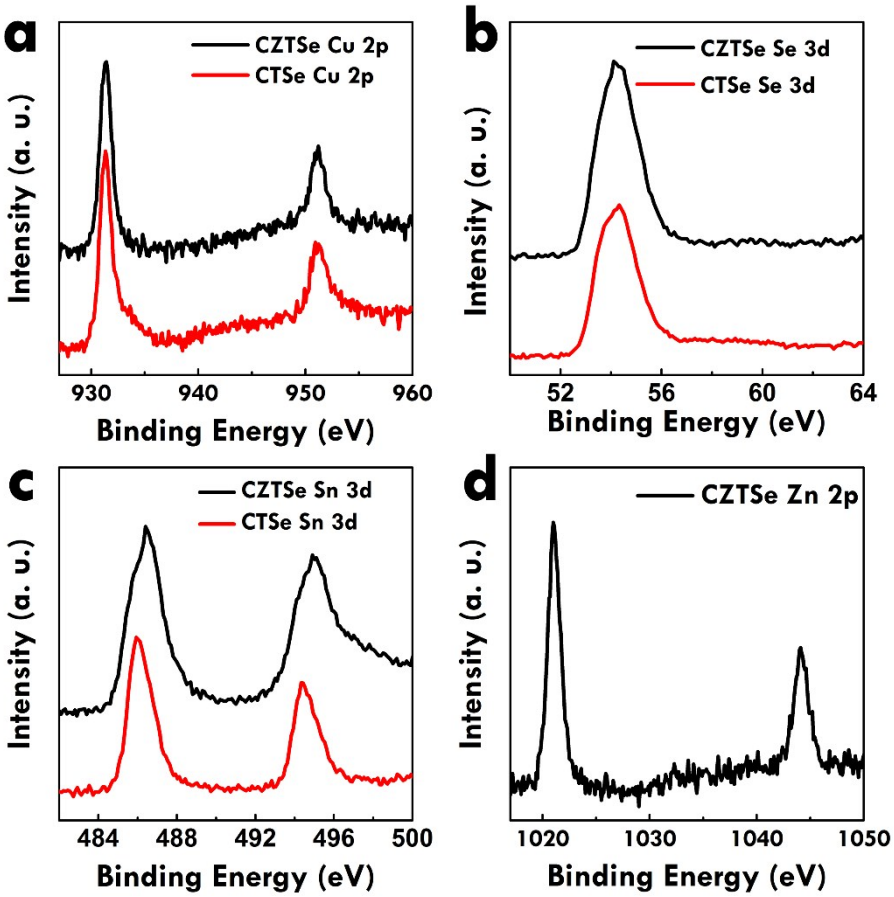

Fig. S4. XPS spectra of (a) Cu 2p, (b) Se 3d, (c) Sn 3d, and (d) Zn 2p of CZTSe (black line) and CTSe (red line).

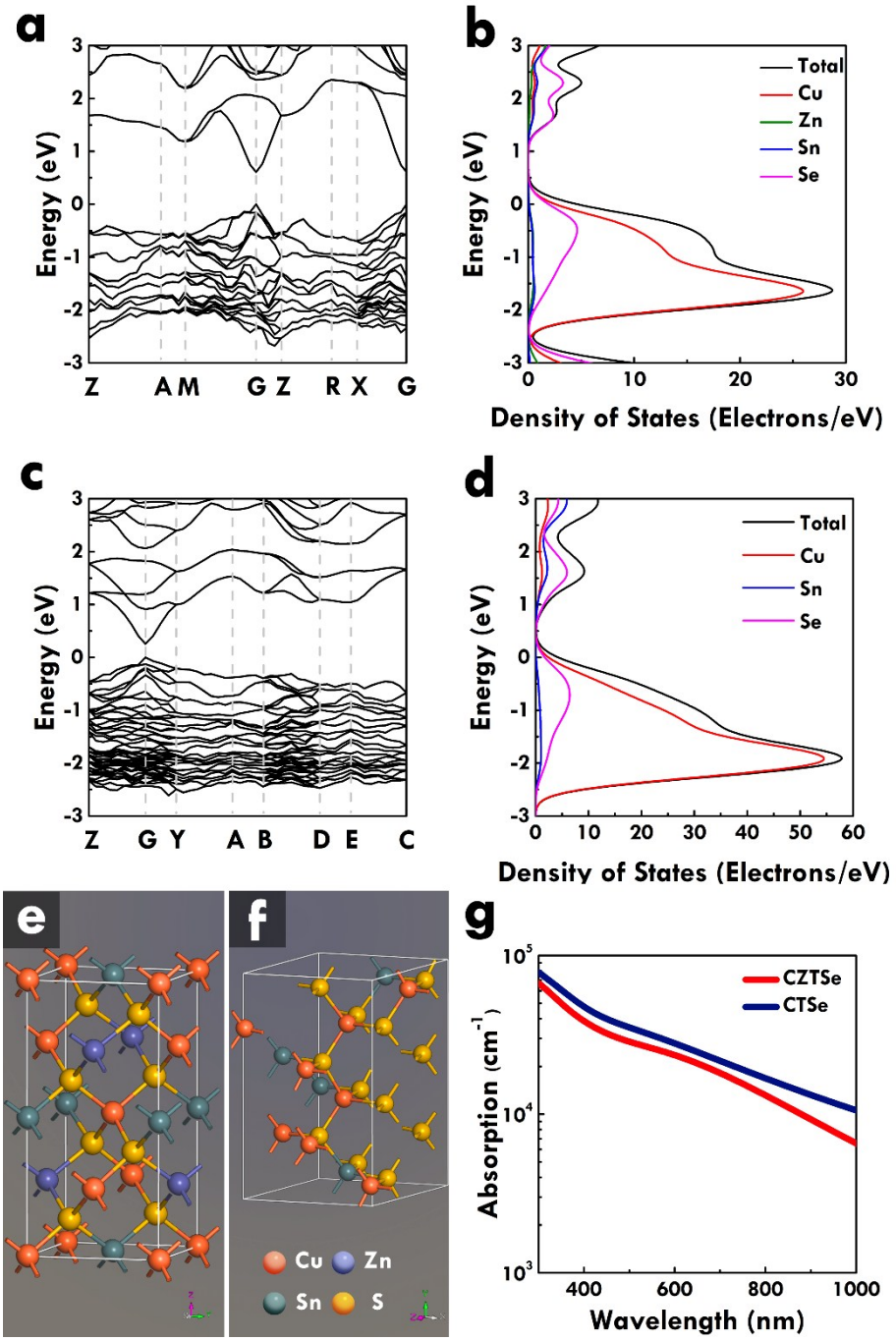

Fig. S5. Electronic band structure and PDOS/DOS of (a, b) CZTSe and (c, d) CTSe. Schematic representations of (e) CZTSe and (f) CTSe unit cell. (g) Absorption coefficients of CZTSe (red line) and CTSe (blue line).

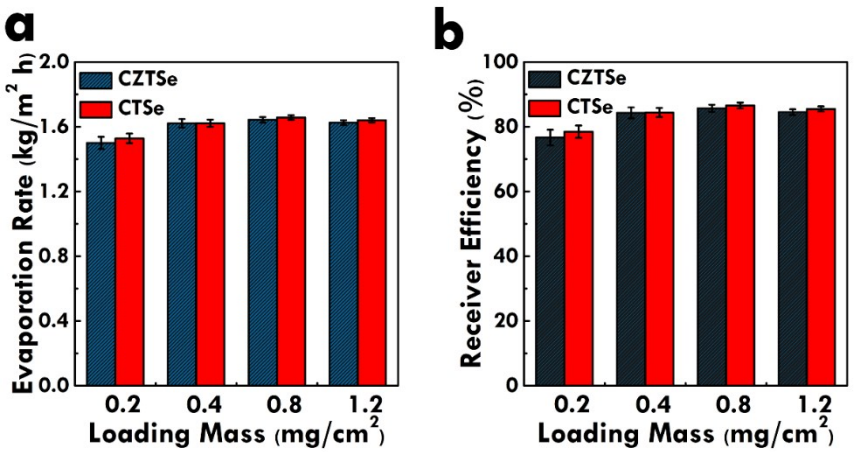

Fig. S6. Optimal experiments (a) evaporation rates and (b) solar thermal conversion efficiencies of different CZTSe (black column) and CTSe (red column) loading masses.

Table S1. Solar water evaporation based on hydrophilic/hydrophobic nanoporous double layer membrane in this work compared with other materials and designs under one Sun.

Sample	Hydropathy	Evaporation rate (kg/m^2 h)	Efficiency (%)	Desalination testing	Salt-rejection ability	Ref.
Carbon based DLS	All-hydrophilic	1.2	64	No	-	1
Au NP/NPT	All-hydrophilic	~1*	~64	No	-	2
Ti_2O_3 NP	All-hydrophilic	1.32	-	No	-	3
MXene Ti_3C_2	All-hydrophilic	1.33*	84	No	-	4
3D-CG/GN	All-hydrophilic	1.25*	85.6	No	-	5
rGO/PU	All-hydrophilic	0.9*	65	No	-	6
Carbonized mushroom	All-hydrophilic	1.475	78	No	-	7
GO-based aerogels	All-hydrophilic	1.622	83	No	-	8
Artificial tree	All-hydrophilic	1.08*	74	No	-	9
TiAlON/NiO	All-hydrophilic	1.13*	73	No	-	10
Wood/CNT	All-hydrophilic	0.95*	65	No	-	11
Al NP/AAM	All-hydrophilic	1*	58	Yes	Not mentioned	12
GO with 2D water path	All-hydrophilic	1.45	80	Yes	Not mentioned	13
Plasmonic wood	All-hydrophilic	~1.0*	~67	Yes	Microchannels (Intermittent working)	14
Tree-inspired design	All-hydrophilic	~0.8*	57.3	Yes	Microchannels (Intermittent working)	15
SWCNT/MoS_2	All-hydrophilic	~1.1*	81	Yes	Not mentioned	16
Hierarchical graphene foam	All-hydrophilic	1.4*	91.4	Yes	Washing (Intermittent working)	17
VA-GSM	All-hydrophilic	1.62	86.5	Yes	Not mentioned	18
3DG	All-hydrophilic	1.30*	87.04	Yes	Not mentioned	19
Porous N-doped graphene	N-doping enhance the wettability	1.5	80	No	-	20
PPy-coated SS mesh	All-hydrophobic	0.92*	58	No	-	21
GDY/CuO	All-hydrophobic	1.55	91	No	-	22
Cu_2SnSe_3 hierarchical nanosphere arrays	**Hydrophilic/ hydrophobic nanoporous double layer**	**1.657 1.381***	**86.6**	**Yes**	**Hydrophobic effect (Continuous working)**	**This work**

* Dark evaporation rate excluded.

References

1. H. Ghasemi, G. Ni, A. M. Marconnet, J. Loomis, S. Yerci, N. Miljkovic and G. Chen, *Nat. Commun.*, 2014, **5**, 4449.
2. L. Zhou, Y. Tan, D. Ji, B. Zhu, P. Zhang, J. Xu, Q. Gan, Z. Yu and J. Zhu, *Sci. Adv.*, 2016, **2**, e1501227.
3. J. Wang, Y. Li, L. Deng, N. Wei, Y. Weng, S. Dong, D. Qi, J. Qiu, X. Chen and T. Wu, *Adv. Mater.*, 2017, **29**, 1603730.
4. R. Li, L. Zhang, L. Shi and P. Wang, *ACS Nano*, 2017, **11**, 3752-3759.
5. Y. Li, T. Gao, Z. Yang, C. Chen, W. Luo, J. Song, E. Hitz, C. Jia, Y. Zhou, B. Liu, B. Yang and L. Hu, *Adv. Mater.*, 2017, **29**, 1700981.
6. G. Wang, Y. Fu, A. Guo, T. Mei, J. Wang, J. Li and X. Wang, *Chem. Mater.*, 2017, **29**, 5629-5635.
7. N. Xu, X. Hu, W. Xu, X. Li, L. Zhou, S. Zhu and J. Zhu, *Adv. Mater.*, 2017, **29**, 1606762.
8. X. Hu, W. Xu, L. Zhou, Y. Tan, Y. Wang, S. Zhu and J. Zhu, *Adv. Mater.*, 2017, **29**, 1604031.
9. H. Liu, C. Chen, G. Chen, Y. Kuang, X. Zhao, J. Song, C. Jia, X. Xu, E. Hitz, H. Xie, S. Wang, F. Jiang, T. Li, Y. Li, A. Gong, R. Yang, S. Das and L. Hu, *Adv. Energy Mater.*, 2018, **8**, 1701616.
10. H. Liu, X. Zhang, Z. Hong, Z. Pu, Q. Yao, J. Shi, G. Yang, B. Mi, B. Yang, X. Liu, H. Jiang and X. Hu, *Nano Energy*, 2017, **42**, 115-121.
11. C. Chen, Y. Li, J. Song, Z. Yang, Y. Kuang, E. Hitz, C. Jia, A. Gong, F. Jiang, J. Y. Zhu, B. Yang, J. Xie and L. Hu, *Adv. Mater.*, 2017, **29**, 1701756.
12. L. Zhou, Y. Tan, J. Wang, W. Xu, Y. Yuan, W. Cai, S. Zhu and J. Zhu, *Nat. Photon.*, 2016, **10**, 393-398.
13. X. Li, W. Xu, M. Tang, L. Zhou, B. Zhu, S. Zhu and J. Zhu, *Proc. Natl. Acad. Sci.*, 2016, **113**, 13953-13958.
14. M. Zhu, Y. Li, F. Chen, X. Zhu, J. Dai, Y. Li, Z. Yang, X. Yan, J. Song, Y. Wang, E. Hitz, W. Luo, M. Lu, B. Yang and L. Hu, *Adv. Energy Mater.*, 2018, **8**, 1701028.
15. M. Zhu, Y. Li, G. Chen, F. Jiang, Z. Yang, X. Luo, Y. Wang, S. D. Lacey, J. Dai, C. Wang, C. Jia, J. Wan, Y. Yao, A. Gong, B. Yang, Z. Yu, S. Das and L. Hu, *Adv. Mater.*, 2017, **29**, 1704107.
16. X. Yang, Y. Yang, L. Fu, M. Zou, Z. Li, A. Cao and Q. Yuan, *Adv. Funct. Mater.*, 2018, **28**, 1704505.
17. H. Ren, M. Tang, B. Guan, K. Wang, J. Yang, F. Wang, M. Wang, J. Shan, Z. Chen, D. Wei, H. Peng and Z. Liu, *Adv. Mater.*, 2017, **29**, 1702590.
18. P. Zhang, J. Li, L. Lv, Y. Zhao and L. Qu, *ACS Nano*, 2017, **11**, 5087-5093.
19. Y. Yang, R. Zhao, T. Zhang, K. Zhao, P. Xiao, Y. Ma, P. M. Ajayan, G. Shi and Y. Chen, *ACS Nano*, 2018, **12**, 829-835.
20. Y. Ito, Y. Tanabe, J. Han, T. Fujita, K. Tanigaki and M. Chen, *Adv. Mater.*, 2015, **27**, 4302-4307.
21. L. Zhang, B. Tang, J. Wu, R. Li and P. Wang, *Adv. Mater.*, 2015, **27**, 4889-4894.
22. X. Gao, H. Ren, J. Zhou, R. Du, C. Yin, R. Liu, H. Peng, L. Tong, Z. Liu and J. Zhang, *Chem. Mater.*, 2017, **29**, 5777-5781.

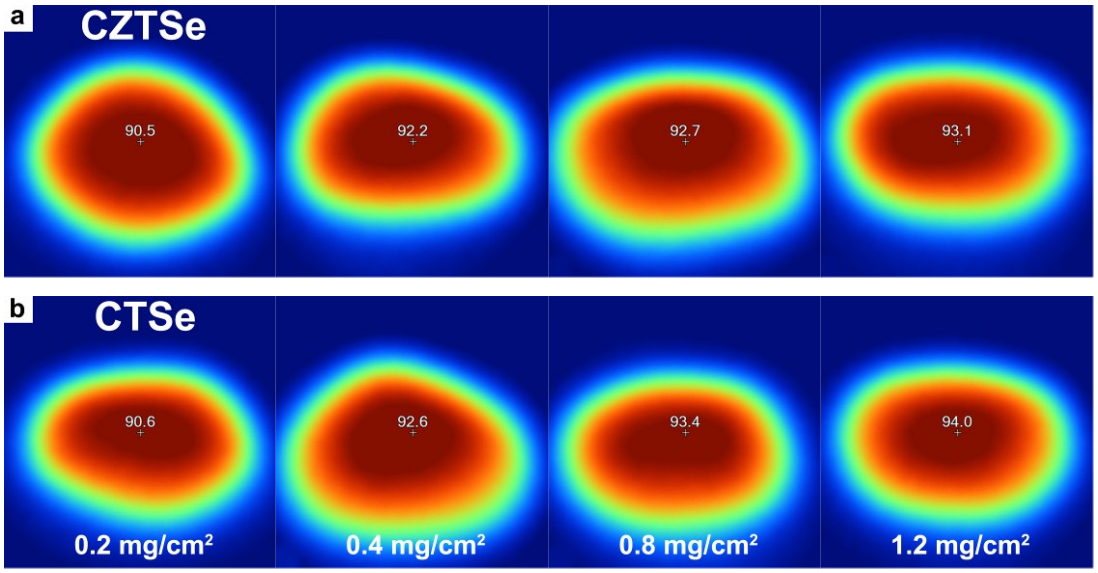

Fig. S7. IR images of (a) CZTSe and (b) CTSe membranes with different loading masses directly exposed on one Sun irradiation for 5 min.

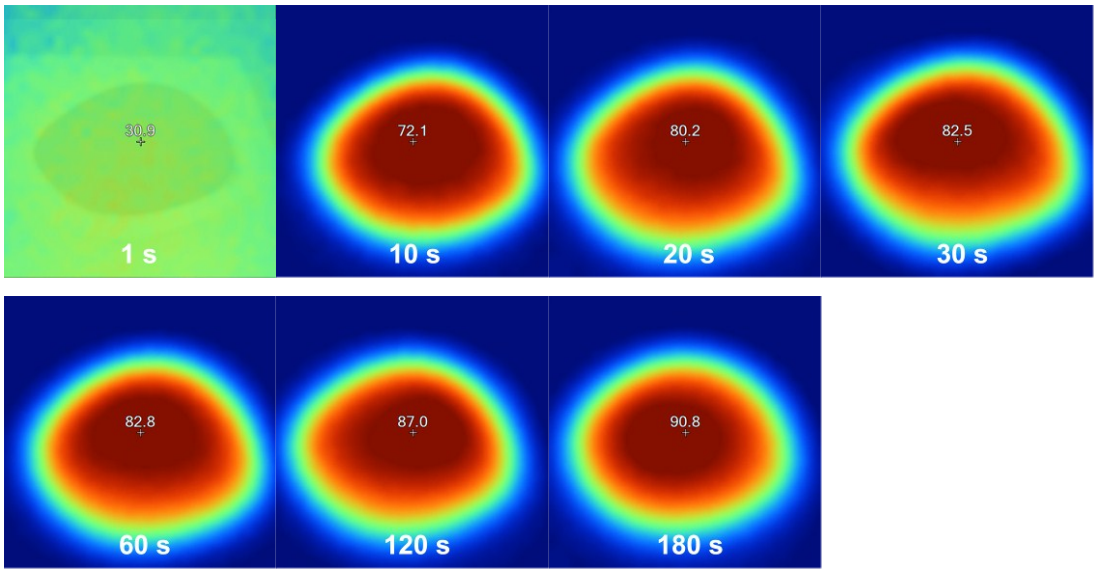

Fig. S8. IR images of CTSe membrane (loading mass: 0.8 mg/cm^2) directly exposed on one Sun irradiation for 1, 10, 20, 30, 60, 120 and 180 s.

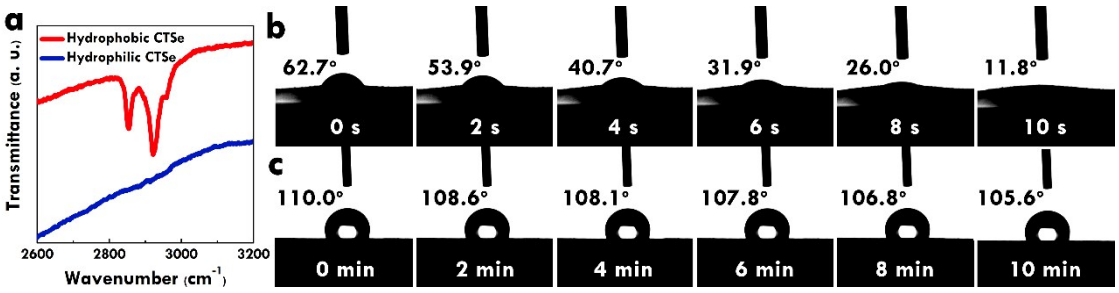

Fig. S9. (a) FTIR spectra of hydrophobic (red line) and hydrophilic (blue line) CTSe nanospheres. Time course contact angles of (b) hydrophilic and (c) hydrophobic CTSe membranes.

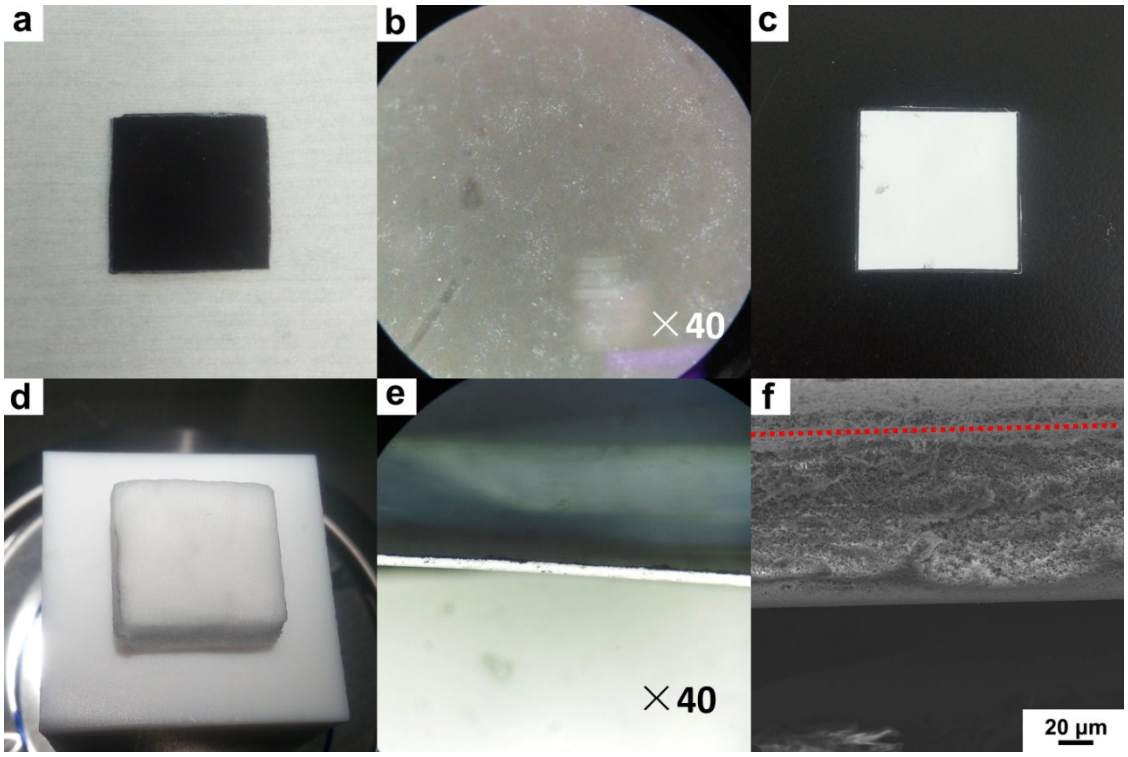

Fig. S10. Optical photos of HHNDL membrane (a and b) top and (c) bottom surfaces, and (d) nonwoven fabrics surface after continuous 15 day running. (e) Optical photo and (f) SEM image of the hydrophilic/hydrophobic interface after continuous 15 day running.

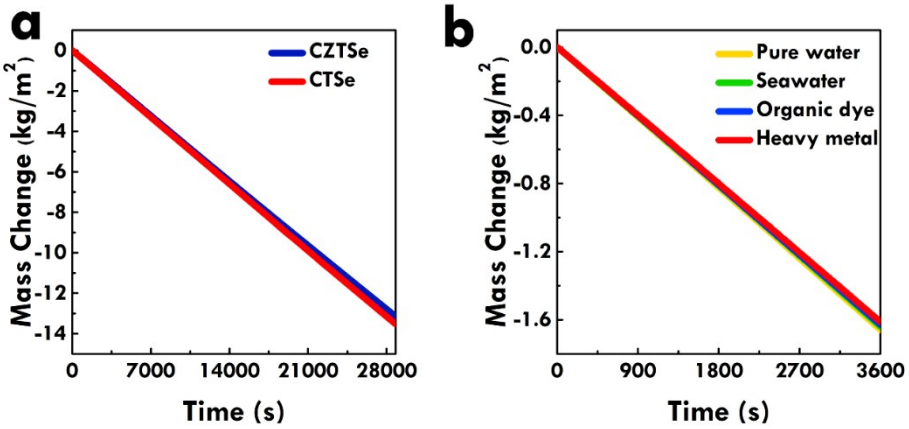

Fig. S11. (a) Evaporation stability of CZTSe (blue line) and CTSe (red line) membranes for 8 h. (b) Mass change of different water samples: pure water, seawater (Bohai Sea), organic dye solution (10 mg/L RhB) and heavy metal solution (0.5 mM $K_2Cr_2O_7$).

Table S2. Concentration of Cu and Se elements in bulk seawater and vapor after solar desalination.

Water sample	Bulk seawater (mg/L)	Vapor/condensed water (mg/L)
Cu	0.00	0.00
Se	0.00	0.00

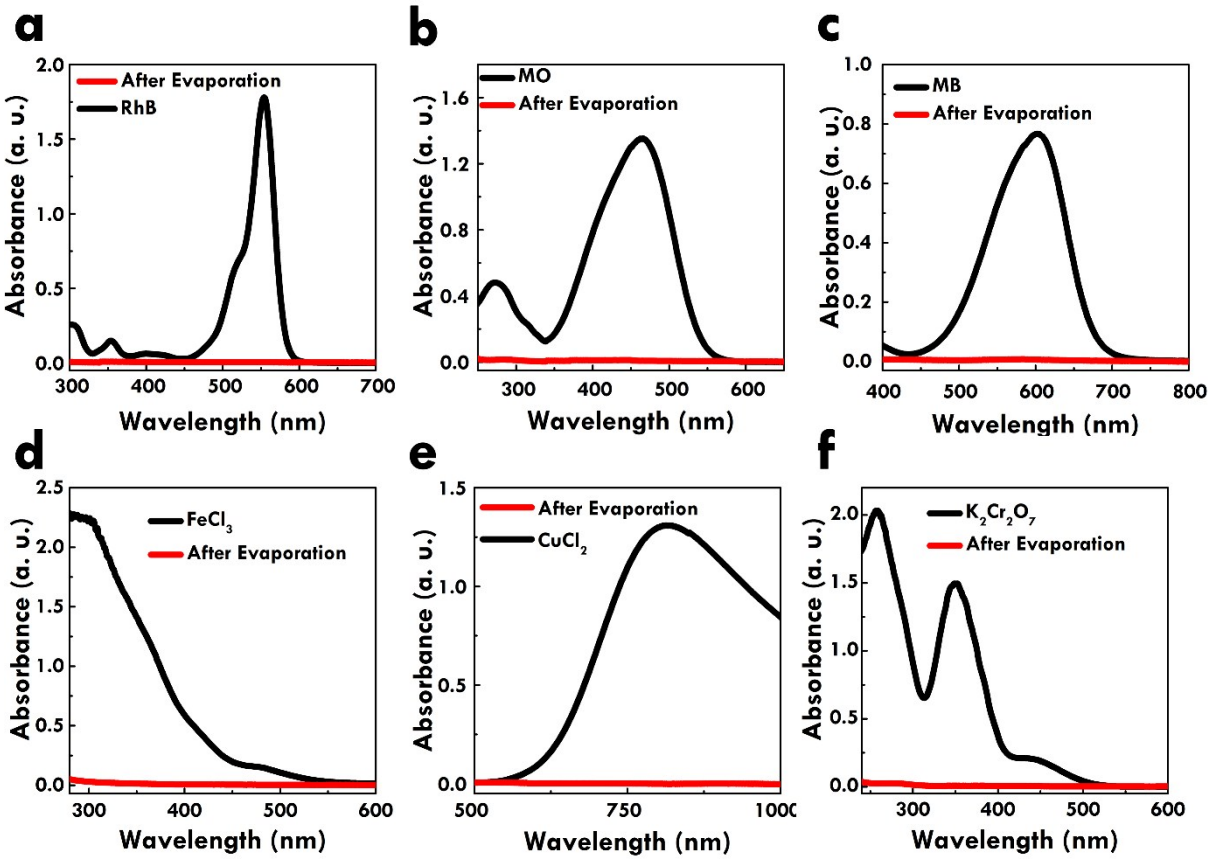

Fig. S12. Absorption spectra of (a) RhB, (b) MO, (c) MB, (d) $FeCl_3$, (e) $CuCl_2$ and (f) $K_2Cr_2O_7$ solutions before (black line) and after (red line) evaporation.

Author contributions

Y. Y. and H. Z. contributed equally to this work. W. Q. and Y. D. proposed the whole research direction and guided the project. Y. Y., H. Z., J. Z. and D. Y. designed and performed the fabrication and characterization experiments. Y. L. and B. L. conducted the anti-bacteria experiments. All authors analyzed the experimental results and drafted the manuscript.